Intravascular Ultrasound Assessment of In-Stent Restenosis in Saphenous Vein Grafts

Rafal Wolny, MD, PhD[a,b,c], Gary S. Mintz, MD[b], Mitsuaki Matsumura, BS[b], Masaru Ishida, MD[b,c], Yuqi Fan, MD[b,c,d], Khady N. Fall, MD, MPH[c], Manish A. Parikh, MD[b,c], LeRoy E. Rabbani, MD[b,c], Ziad A. Ali, MD, DPhil[b,c], Dimitri Karmpaliotis, MD, PhD[b,c], Ajay J. Kirtane, MD, SM[b,c], Jeffrey W. Moses, MD[b,c,e], and Akiko Maehara, MD[b,c,*]

Outcomes after percutaneous coronary interventions (PCI) in saphenous vein grafts (SVG) are inferior compared with native coronary arteries, but the mechanisms of SVG in-stent restenosis (ISR) have not been well-described. Thus, we aimed to evaluate the patterns of SVG ISR using intravascular ultrasound (IVUS) in 54 SVG ISR lesions. Stent underexpansion was defined as minimum stent area (MSA) <5 mm^2. The time from stent implantation to presentation with ISR (9 BMS, 18 first-generation DES, and 27 second-generation DES) was 3.7 ± 3.0 years. IVUS-defined ISR patterns were categorized as mechanical (33%) or biological (67%). Mechanical patterns comprised 10 cases of stent underexpansion (MSA = 4.2 ± 0.9 mm^2), 6 stent fractures or deformations, and 2 uncovered aorto-anastomotic lesions. Biological patterns comprised 19 cases of neoatherosclerosis, 13 excessive neointimal hyperplasia (NIH, 65 ± 11%), and 4 thrombi. Compared with biological patterns of ISR, mechanical patterns were more frequently located at the SVG anastomosis (72% vs 39%, p = 0.04) and at the SVG hinge motion site (55% vs 21%, p = 0.02). Although patients with mechanical patterns of ISR presented earlier than those with biological patterns (2.3 vs 4.4 years, p = 0.009), 61% of them were diagnosed >1 year after stent implantation. In conclusion, SVG ISR is dominated by biological patterns including neoatherosclerosis. Mechanical patterns of SVG ISR are associated with earlier presentation and location at graft anastomosis or hinge motion site. **(Am J Cardiol 2019;123:1052−1059)**

Native vessel percutaneous coronary intervention (PCI) is the recommended revascularization strategy in patients with saphenous vein graft (SVG) disease because of periprocedural complications and long-term failure associated with vein graft PCI[1,2]; however, unfavorable native vessel anatomy, including a high prevalence of chronic total occlusions (CTO), despite recent developments of advanced CTO recanalization techniques, frequently makes PCI to the SVG the only available revascularization strategy. High rates of target vessel failure (approximately 20% at 1 year) and no clear benefit of drug-eluting stents (DES) over bare metal stents (BMS) suggest different response to stenting of SVGs compared with native coronary arteries.[3] Contrary to native coronary in-stent restenosis (ISR), patterns of SVG ISR remain to be clarified. Therefore, the aim of our study was to use intravascular ultrasound (IVUS) to assess patterns of SVG ISR.

Methods

This was a retrospective, observational, single-center study at NewYork-Presbyterian Hospital/Columbia University Medical Center (New York, New York). Between January 1, 2007, and September 30, 2017, IVUS was performed to 368 SVGs, including 105 ISR lesions, out of which we identified 54 lesions (51 patients) with analyzable IVUS images that were obtained before any intervention or after pre-dilatation with ≤2.0 mm balloon. ISR was defined as >50% luminal diameter stenosis assessed by angiography or IVUS minimum lumen cross-sectional area (MLA) <4 mm^2 either in-stent or within 5 mm proximal or distal to the stent edges. The study was approved by the institutional review board of Columbia University Medical Center.

Quantitative and qualitative angiographic analysis was performed by 2 experienced analysts blinded to clinical and IVUS findings (M.I. and Y.F.) using QAngioXA (Medis, Leiden, the Netherlands) according to standardized methodology.[4] Angiographic restenosis was classified in the worst view as: (i) focal, ≤10 mm in length which was further divided into stent edge or stent body; (ii) diffuse, ≥10 mm in length within the stent; and (iii) proliferative, ≥10 mm in length and extending beyond the stent edges.[5] The primary assessment of a hinge motion was qualitative (defined as presence of any hinge motion within the ISR lesion), done by agreement of 3 analysts. Additionally, a maximum hinge motion angle was measured in all lesions by an independent reader according to the methodology described by Ino et al.[6] Briefly, the maximum and minimum SVG angulation

[a]Institute of Cardiology, Warsaw, Poland; [b]Clinical Trials Center, Cardiovascular Research Foundation, New York, New York; [c]Division of Cardiology, Department of Medicine, NewYork-Presbyterian Hospital/Columbia University Medical Center, New York, New York; [d]Department of Cardiology, Shanghai 9th People's Hospital, Shanghai JiaoTong University School of Medicine, Shanghai, China; and [e]St. Francis Hospital, Roslyn, New York. Manuscript received November 30, 2018; revised manuscript received and accepted December 19, 2018.

See page 1058 for disclosure information.

*Corresponding author: Tel: (646) 434-4500.

E-mail address: amaehara@crf.org (A. Maehara).

0002-9149/
https://doi.org/10.1016/j.amjcard.2018.12.030

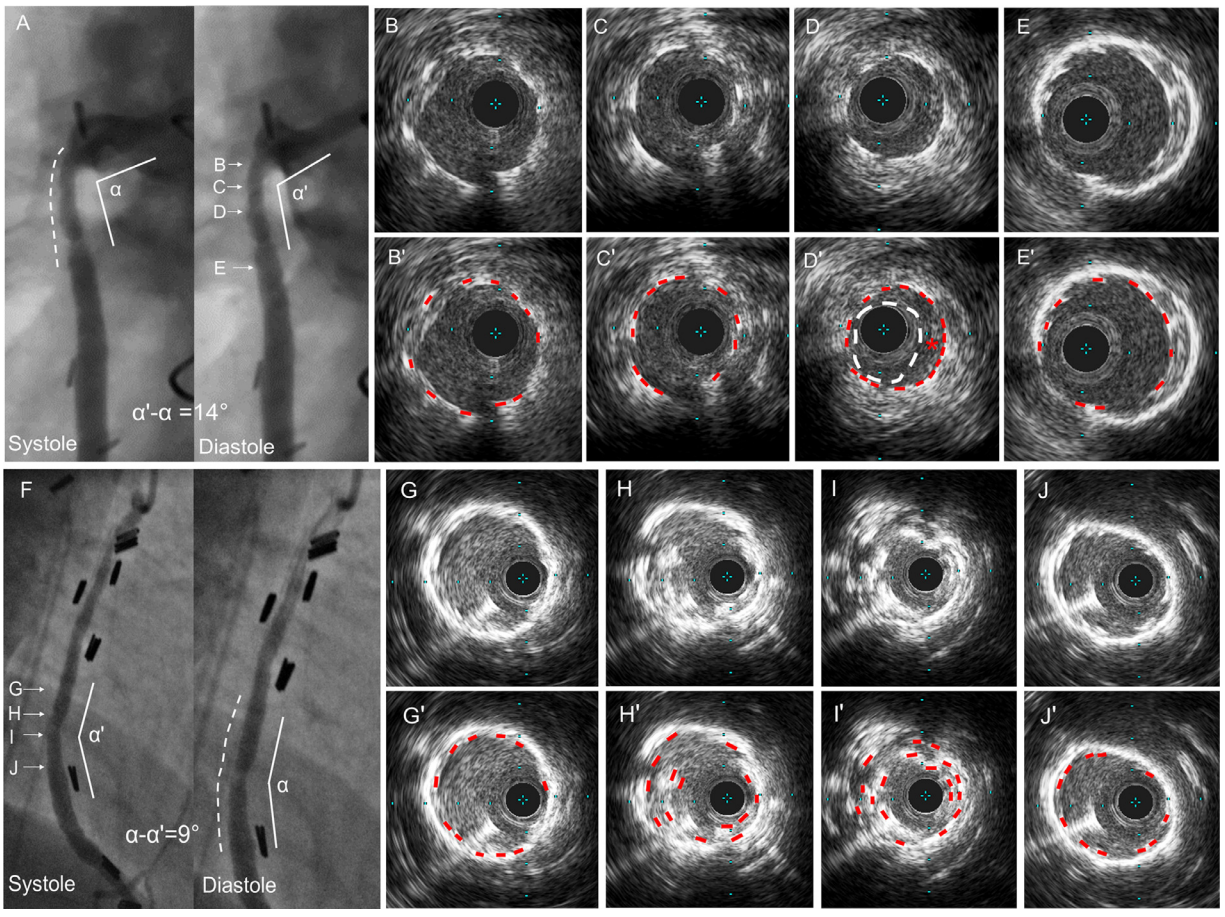

Figure 1. **Examples of late saphenous vein graft in-stent restenosis at the site of a hinge motion caused by A) stent underexpansion and B) stent deformation.**

(A) Coronary angiogram shows an ISR lesion in the proximal SVG to the right coronary artery 4.5 years postimplantation of a bare metal stent (white dashed line) at a hinge motion site with corresponding IVUS cross sections (B−E). The red dashed line shows the old stent, and white dashed line shows the lumen (B′−E′). The MSA measured 4.5 mm^2 along with a focal neointimal hyperplasia (red asterisk) (D′) resulting in a minimum lumen area of 2.3 mm^2. Stent cross-sectional area proximal to the MSA measured 6.8 mm^2 (B') and distal to the MSA measured 7.1 mm^2 (E').

(F) Coronary angiogram shows an ISR lesion in the middle SVG to the right coronary artery 4 years postimplantation of a single drug-eluting stent (dashed line) at a hinge motion site with corresponding IVUS cross-sections (G−J). The red dashed line shows the old stent (G'−J'). In the middle of the stent there is stent deformation defined as multiple stent strut layers when only a single layer should be seen (H', I'), the MSA measured 2.8 mm^2 (I'). The stent area proximal and distal to the deformation site measured 9.9 mm^2 (G') and 8.1 mm^2 (J').

(ISR = in-stent restenosis; IVUS = intravascular ultrasound; MSA = minimum stent area; SVG=saphenous vein graft).

within the ISR lesion during cardiac cycle was measured, and Δ angle was calculated (Figure 1).

IVUS was performed using rotational catheters (40-MHz Atlantis/Opticross, Boston Scientific, Maple Grove, Minnesota; 45-MHz Revolution, Philips, San Diego, California; or 60-MHz Kodama HD, ACIST, Eden Prairie, Minnesota) and motorized pullback at 0.5 to 1.0 mm/s. Predilation with a small balloon was required in 12 (22%) lesions before imaging. IVUS analysis was performed by consensus of 3 experienced readers (R.W., M.M., and A.M.) using planimetry software (echoPlaque 4.0, INDEC Medical Systems, Los Altos, California) and included cross-sectional area (CSA) measurements of the lumen, stent, and vessel at MLA and minimum stent CSA (MSA) sites as well as proximal and distal references. Vessel area was defined as the outer border of the SVG sonolucent zone.[7] Reference sites were defined as mostly healthy cross sections within 5 mm proximal and distal to the stent. For lesions located at aortic or distal anastomoses, only 1 (distal) reference segment was used. The following definitions were applied:

- NIH CSA = stent−lumen CSA.
- Plaque burden = (vessel−lumen)/vessel CSA (in restenotic segment the stent area was used instead of lumen area)
- Vessel remodeling index = vessel CSA at MLA/average of proximal and distal reference vessel CSA
- Stent expansion = MSA/average reference lumen CSA
- Stent underexpansion: MSA <5 mm^2.[8]
- Neoatherosclerosis: calcified neointima (or calcified neointima nodule) or attenuated or ruptured neointima. Calcium was defined as hyperechoic neointima with acoustic shadowing, calcified nodule as an irregular convex-shaped neointima with underlying calcified plaque,[9] attenuated neointima as ultrasound shadowing of the stent despite the absence of superficial calcium, plaque

rupture as neointimal cavity communicating with the lumen,[10] and thrombus as either irregular pedunculated intraluminal mass or microchannels.[11]
- Complete stent fracture: separation of the stent into 2 pieces by image slices with no visible stent struts.
- Partial stent fracture: absence of stent struts ≥1/3 of the stent circumference with separation of proximal and distal fragments or ≥1/3 of stent circumference with double layer of struts within a single stent.[12]
- Longitudinal stent deformation: multiple layers of stent struts seen in any single cross section within a single stent, typically located at the aorto-anastomosis.

Uncovered ostium: an SVG stenosis within 5 mm proximal to a stent implanted to treat an aorto-anastomotic lesion, in which MLA is located outside the stent.

The primary patterns of ISR were classified as (1) mechanical (stent underexpansion, stent fracture or deformation, or uncovered ostium) or (2) biological (NIH, neoatherosclerosis, or thrombus). In case of >1 possible cause, the primary pattern was decided as follows:

- When 2 findings were present, the 1 causing smaller lumen area was considered primary.
- When neointima was found exclusively at the site of stent underexpansion, fracture, or deformation, the mechanical finding was considered primary.
- Stent fracture or deformation was always considered the primary cause of failure when found within 5 mm proximal or distal to the MLA site.
- When both homogeneous neointima and any component of neoatherosclerosis were found, neoatherosclerosis was considered primary.

The analyses were conducted using SPSS version 22.0 (IBM, Armonk, New York). Categorical variables were presented as count and percentage and compared with the χ^2 or Fisher exact test, as appropriate. Normally distributed continuous variables were compared with the paired Student *t* test, and non-normally distributed continuous variables were compared with the nonparametric Mann-Whitney *U* test. Two-sided p <0.05 was considered statistically significant.

Results

Three patients presented at 2 timepoints due to independent lesions in different SVGs. Finally, 54 SVG ISR lesions in 51 patients were included. Mean age was 72.4 ± 10.4 years old, 78% were men and 50% presented with unstable angina. Clinical characteristics at the time of ISR are summarized in Table 1. SVG age was 16.0 ± 7.4 years. In 19 (35%) lesions the indication for previous PCI was ISR. Restenotic stents included 9 (17%) BMS, 18 (33%) first-generation DES, and 27 (50%) second-generation DES. Duration from stent implantation to presentation with ISR was 3.7 ± 3.0 years and was longest in BMS, followed by first- and second-generation DES (5.3 ± 3.5 years, 4.1 ± 3.0 years, and 2.9 ± 2.6 years, respectively). Twelve patients (22%) presented within 1 year from the index PCI.

Most lesions (36, 67%) had a biological pattern of ISR, including 13 (24%) excessive NIH, 19 (35%) neoatherosclerosis, and 4 (7%) thrombi. A mechanical pattern of ISR was found in 18 (33%) lesions, including 10 (19%) underexpanded stents, 4 (7%) stent fractures (all with partial strut overlap), 2 (4%) stent deformations, and 2 (4%) uncovered aorto-ostia. In 19 (35%) lesions >1 ISR mechanism was

Table 1
Clinical characteristics, medication, and symptoms at the time of in-stent restenosis

Variable	Overall (n = 54)	Mechanical cause ISR (n = 18)	Biological cause ISR (n = 36)	p
Patient characteristics				
Age (years)	72.4 ± 10.4	71.7 ± 9.7	72.8 ± 11.1	0.91
Men	42 (78%)	15 (83%)	27 (75%)	0.73
Hypertension	48 (89%)	16 (89%)	32 (89%)	1.00
Dyslipidemia	54 (100%)	18 (100%)	36 (100%)	1.00
Diabetes mellitus	23 (43%)	5 (28%)	18 (50%)	0.15
Insulin-treated	9 (17%)	0 (0%)	9 (25%)	0.02
Smoker	27 (50%)	8 (44%)	19 (53%)	0.77
Chronic kidney disease*	21 (39%)	7 (39%)	14 (39%)	1.00
Dialysis	3 (6%)	1 (6%)	2 (6%)	1.00
Clinical presentation at the time of ISR				
Stable coronary artery disease	25 (46%)	6 (33%)	19 (53%)	0.25
Unstable angina	27 (50%)	12 (67%)	15 (42%)	0.15
STEMI and NSTEMI†	2 (4%)	0 (0%)	2 (6%)	0.55
Medication at the time of ISR				
Aspirin	51 (94%)	18 (100%)	33 (92%)	0.54
Thienopyridine	47 (86%)	15 (83%)	31 (86%)	1.00
Angiotensin-converting enzyme inhibitor/angiotensin II receptor blocker	37 (67%)	8 (44%)	28 (78%)	0.03
Statin	50 (94%)	15 (83%)	34 (94%)	0.32

* Defined as estimated glomerular filtration rate <60 mL/min/1.73 m^2 calculated using the Modification of Diet in Renal Disease equation.
† One patient presented with ST-elevation myocardial infarction (STEMI) and one with non−ST-elevation myocardial infarction. ISR = in-stent restenosis.

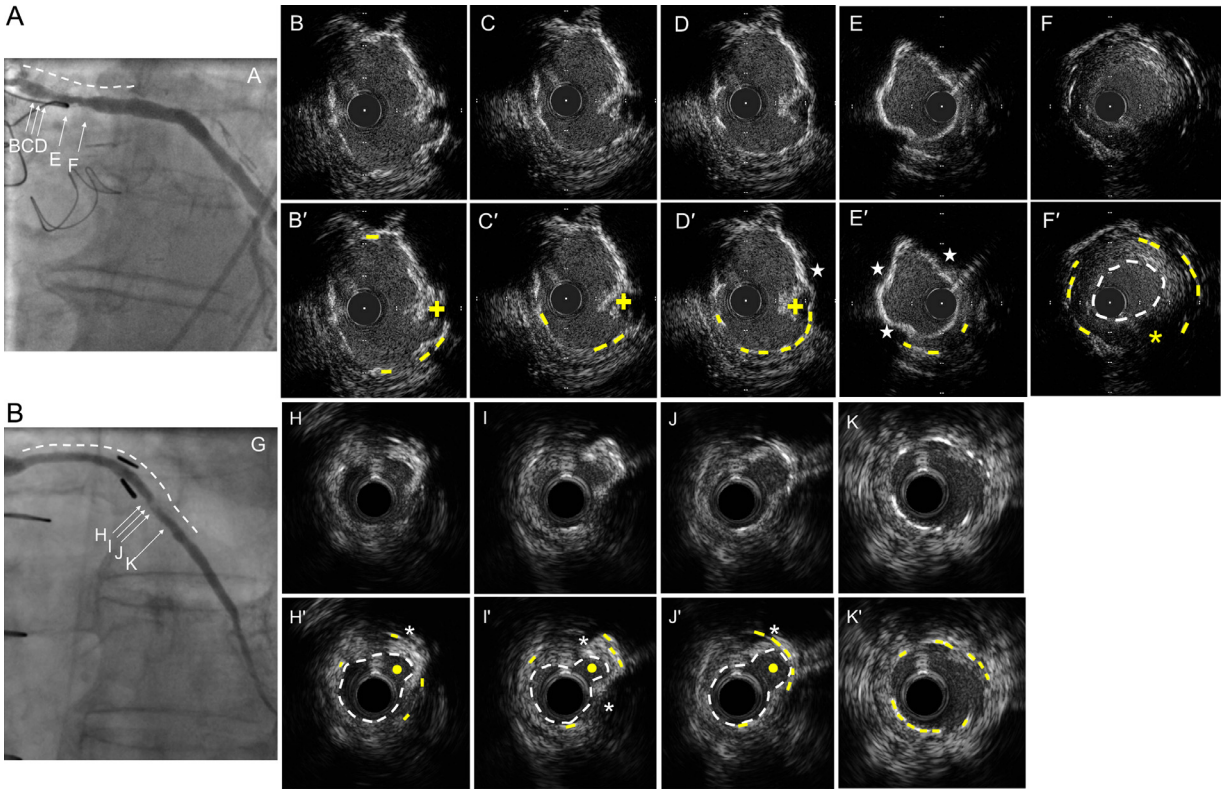

Figure 2. **Example of late saphenous vein graft in-stent restenosis caused by (A) Neoatherosclerosis with calcified and attenuated neointima and (B) Neoatherosclerosis with attenuated and ruptured neointima.**

(A) Coronary angiogram shows a proximal ISR lesion in the SVG to the obtuse marginal 8 years post-implantation of a drug-eluting stent (white dashed line) with corresponding IVUS cross-sections (B−F). The yellow dashed line (B'−F') shows the old stent, and the white dashed line shows the lumen area (F'). The calcified nodule (yellow cross, B'−D') on the top of calcified neointima (white stars, D' and E') and attenuated neointima (white asterisk, F') indicate neoatherosclerosis.

(G) Coronary angiogram shows an ISR lesion in the middle of an SVG to a diagonal branch 4 years postimplantation of 2 bare-metal stents (white dashed line); H-K are the corresponding IVUS cross sections. Yellow dashed lines show old stents, and white dashed lines show lumen area with a rupture cavity (yellow dot) within the attenuated neointima (white asterisk) (H'−J'). The old stent (K') area was 5.3 mm^2 and its expansion was 78%.

(ISR = in-stent restenosis; IVUS = intravascular ultrasound; SVG = saphenous vein graft).

found. Clinical characteristics of patients with mechanical versus biological patterns of ISR were similar, except for a higher prevalence of insulin-dependent diabetes mellitus in the latter group (Table 1). Examples of different IVUS-defined ISR patterns are shown in Figures 1 and 2.

Patients with mechanical patterns of ISR presented earlier compared with biological patterns of ISR (2.3 ± 1.9 years vs 4.4 ± 3.2 years, p = 0.009). Seven (39%) patients with mechanical ISR patterns presented within 1 year from index PCI compared with 5 (14%) patients with biological patterns of ISR (p = 0.04). Patients with stent failure due to uncovered ostium and thrombus presented earliest (1.6 ± 0.4 years and 1.7 ± 1.7 years, respectively), followed by ISR due to stent fracture or deformation, stent underexpansion, and NIH (2.3 ± 2.0 years, 2.4 ± 2.0 years, and 2.4 ± 2.4 years, respectively), whereas the latest presentation was associated with neoatherosclerosis (6.4 ± 2.7 years). All cases of neoatherosclerosis were diagnosed ≥2 years after stenting. When SVG ISR lesions were categorized according to tertile of time to failure, ISR due to NIH was significantly more prevalent in the first compared with the third tertile (37% vs 6%, p = 0.03) (Figure 3A).

There was no difference between the distribution of BMS, first-generation DES, and second-generation DES within mechanical versus biological patterns of SVG ISR (11%, 28%, and 66% vs 19%, 36%, and 45%, respectively; p = 0.49); however, all 6 cases of stent fracture and deformation were found in DES, as well as all 4 cases of thrombus, and all 4 calcified nodules (Figure 3B). Mechanical and biological patterns of ISR were not significantly different in terms of the number (1.3 ± 0.5 vs 1.3 ± 0.7, p = 0.82), total length (25.6 ± 12.7 mm vs 20.0 ± 8.3 mm, p = 0.12), and maximal nominal stent diameter of previously implanted stents (Table 2) as well as SVG age (16.7 ± 8.2 years vs 15.9 ± 7.1 years, p = 0.82, respectively).

Qualitative and quantitative angiographic findings are summarized in Table 2. Mechanical compared with biological patterns of ISR were more frequently located at SVG anastomosis as well as at an SVG hinge motion site. Maximal Δ angle within the lesion was significantly larger in mechanical compared with biological patterns. Other angiographic parameters were not significantly different.

Lesions located at the SVG hinge motion site (n = 20, 37%) were characterized by a larger maximal Δ angle

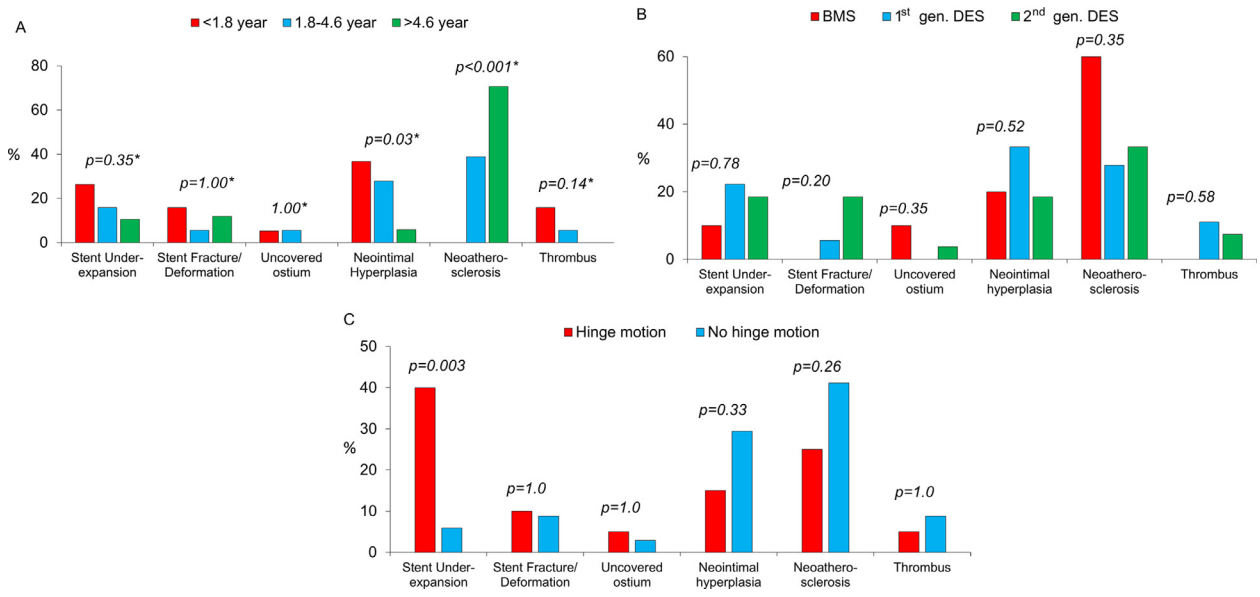

Figure 3. **Intravascular ultrasound-defined in-stent restenosis patterns.**
(A) Tertiles of time to presentation with ISR. SVG ISR in the early tertile (<1.8 years) showed more neointimal hyperplasia; and SVG ISR in the late tertile (>4.6 years) showed more neoatherosclerosis; *p value for a comparison between early (<1.8 years) and late (>4.6 years) tertile. (B) Types of restenotic stents. SVG ISR in bare metal stents showed numerically more neoatherosclerosis in comparison with drug-eluting stents. (C) Presence of hinge motion at the lesion. SVG ISR at a hinge motion site showed more stent underexpansion. (ISR = in-stent restenosis; SVG = saphenous vein graft).

within the lesion (14.3 ± 4.1 vs 3.9 ± 2.4°, p = 0.0001), a higher incidence of stent underexpansion (40% vs 6%, p = 0.003), less %NIH (45% vs 59%, p = 0.02), and worse IVUS-defined stent expansion (70% vs 94%, p = 0.01) compared with lesions located at nonhinge motion sites (Figure 3C). No differences were found between lesions located at a hinge motion site compared with lesions found elsewhere in terms of ISR patterns other than stent underexpansion, duration to stent failure (3.5 ± 2.8 vs 3.9 ± 3.2 years, p = 0.68), SVG age (15.5 ± 7.2 vs 16.4 ± 7.8 years, p = 0.69), MLA (3.0 ± 0.8 vs 2.8 ± 1.1 mm^2, p = 0.43), and MSA (6.2 ± 2.8 vs 7.2 ± 2.9 mm^2, p = 0.21,

Table 2
Angiographic findings according to primary pattern of in-stent restenosis

Variable	Overall (n = 54)	Mechanical cause ISR (n = 18)	Biological cause ISR (n = 36)	p
Grafted vessel				
SVG to right	29 (54%)	10 (56%)	19 (53%)	1.00
SVG to left circumflex	17 (32%)	3 (17%)	14 (39%)	0.13
SVG to left anterior descending	8 (15%)	5 (28%)	3 (8%)	0.10
Lesion location within SVG				
Aorto-anastomosis	24 (44%)	11 (61%)	13 (36%)	0.09
Shaft	27 (50%)	5 (27%)	22 (61%)	0.04
Distal anastomosis	3 (6%)	2 (11%)	1 (3%)	0.26
Nominal stent diameter, mm	3.3 ± 0.5	3.2 ± 0.4	3.3 ± 0.5	0.46
Moderate/severe calcification	4 (7%)	1 (6%)	3 (8%)	1.00
Thrombus	3 (6%)	0 (0%)	3 (8%)	0.54
ISR Pattern				
Focal	43 (80%)	16 (89%)	27 (75%)	0.30
Stent edge	10 (19%)	5 (28%)	5 (14%)	0.27
Stent body	33 (61%)	11 (61%)	22 (61%)	1.00
Diffuse	7 (13%)	1 (6%)	6 (17%)	0.40
Proliferative	4 (7%)	1 (6%)	3 (8%)	1.00
Average reference lumen diameter (mm)	3.0 ± 0.7	2.9 ± 0.4	3.1 ± 0.8	0.50
Minimum lumen diameter (mm)	1.2 ± 0.5	1.2 ± 0.4	1.3 ± 0.5	0.60
Diameter stenosis (%)	59.1 ± 14.1	59.6 ± 12.8	58.4 ± 14.9	0.84
Lesion length (mm)	9.6 ± 5.4	8.5 ± 5.6	10.1 ± 5.3	0.32
Δ Angle within lesion (°)	7.8 ± 5.9	10.4 ± 6.7	6.5 ± 5.1	0.02
Any hinge motion within lesion	20 (37%)	11 (61%)	9 (25%)	0.02

ISR = in-stent restenosis; SVG = saphenous vein graft.

respectively). Examples of mechanical patterns of ISR found at an SVG hinge motion site are shown in Figure 1.

Overall, lesions identified with mechanical patterns of ISR compared with biological patterns were characterized by smaller MSA, worse stent expansion, smaller vessel size at the MLA site, and less %NIH but larger plaque burden behind the stent (Table 3).

Discussion

Key findings of this study are: (1) SVG ISR can be divided into 6 distinct IVUS-defined patterns: NIH, neoatherosclerosis, and thrombosis (biological patterns); and stent underexpansion, stent fracture or mechanical deformation, and uncovered ostium (mechanical patterns). (2) Biological patterns represent the majority of SVG ISR and are associated with later clinical presentation versus mechanical patterns. (3) Mechanical patterns are associated with stent implantation at the SVG aorto-ostial or distal anastomosis or at an SVG hinge motion site.

SVG ISR lesions evaluated in the present study were diagnosed on average 3.7 years after stent implantation—earlier in lesions with mechanical versus biological patterns (2.3 and 4.4 years, respectively) and in DES compared with BMS (3.4 and 5.4 years, respectively). Within dominant biological ISR patterns, neoatherosclerosis was observed later than "pure" NIH (6.4 and 2.4 years, respectively). This observed duration from stenting to ISR presentation was longer in comparison with reported native coronary artery ISR, which occurs on average between 1 and 2 years after DES implantation.[13–15] One explanation for later presentation of SVG ISR (compared with native coronaries) is that larger SVG diameters allow implantation of larger stents that can accommodate a greater volume of neointima before symptom-onset. Another is the common occurrence of neoatherosclerosis as a cause of SVG ISR.

Two-thirds of studied lesions had a biological pattern of ISR: NIH, neoatherosclerosis, or thrombosis. This is in line with previous IVUS analyses of native coronary ISR, reporting NIH-dominant patterns in 59% and 75%.[13,14] Neoatherosclerosis was found in one-third of all lesions (and in 53% of biological patterns of ISR) both in BMS and DES. This corresponds to the results of a histopathological study of native coronary ISR by Nakazawa et al.,[16] who found features of neoatherosclerosis in 31% of DES (n = 209) and 16% of BMS (n = 197). In a recent OCT analysis confined to second-generation DES (n = 171), Song et al.[17] reported neoatherosclerosis in 25% of all ISR; however, OCT is a more sensitive technique to identify neoatherosclerosis compared with IVUS; therefore, it is likely that the prevalence of neoatherosclerosis in SVG ISR is even higher than reported in the current study. In-stent thrombi were found exclusively in DES, supporting the role of late stent thrombosis as a cause of SVG stent failure.

Stent underexpansion was a major cause of ISR in <20% of analyzed lesions. Recently, the reported frequency of IVUS-defined underexpansion among native coronary ISR was 29% to 38% in DES and 59% to 62% in BMS.[13,18] The lower observed prevalence of underexpansion in SVG compared with native coronary ISR may be explained by

Table 3
Intravascular ultrasound findings according to the main pattern of in-stent restenosis

		Mechanical pattern of ISR (n = 18)			Biological pattern of ISR (n = 36)				
Variable	Overall	Under expansion (n = 10)	Stent fracture/ deformation (n = 6)	Uncovered ostium (n = 2)	Overall	NIH (n = 13)	Neoathero sclerosis (n = 19)	Thrombus (n = 4)	p (mechanical vs. biological)
Minimum lumen area (mm^2)	3.0 ± 0.9	3.1 ± 0.8	3.0 ± 1.1	2.5 ± 0.3	2.8 ± 1.0	3.2 ± 1.1	2.4 ± 0.8	3.5 ± 0.8	0.48
Vessel CSA at MLA (mm^2)	12.9 ± 2.5	12.3 ± 1.9	14.6 ± 2.2	10.2 ± 2.1	16.1 ± 5.1	17.7 ± 3.9	14.9 ± 5.5	16.0 ± 4.1	0.02
Area stenosis (%)	58.9 ± 11.0	60.3 ± 9.9	62.1 ± 9.8	45.4 ± 3.8	63.1 ± 13.9	61.6 ± 17.2	64.4 ± 11.3	62.8 ± 8.9	0.30
Minimum stent CSA (mm^2)	4.6 ± 1.0	4.2 ± 0.9	4.4 ± 0.6	5.3 ± 0.2	8.0 ± 2.9	7.9 ± 2.0	7.1 ± 3.1	6.6 ± 1.4	<0.001
Stent expansion (%)	67.5 ± 24.5	55.8 ± 13.9	67.0 ± 13.7	116.4 ± 1.3	92.3 ± 32.5	98.3 ± 34.1	93.1 ± 30.2	71.4 ± 21.8	0.01
>1 stent layer	7 (39%)	5 (50%)	2 (33%)	0 (0%)	11 (31%)	6 (46%)	3 (16%)	2 (50%)	0.56
Maximum NIH (%)	34.0 ± 16.9	27.1 ± 15.8	38.9 ± 12.4	53.9 ± 4.6	63.9 ± 15.1	64.9 ± 10.7	64.9 ± 14.0	52.3 ± 22.9	<0.001
Plaque burden behind stent at MLA (%)	62.7 ± 12.2	63.9 ± 11.7	66.7 ± 5.8	45.0 ± 9.8	49.9 ± 10.1	47.5 ± 7.5	51.0 ± 10.9	53.7 ± 10.6	<0.001
Remodeling index	1.0 ± 0.4	0.8 ± 0.1	1.3 ± 0.4	1.1 ± 0.0	1.1 ± 0.5	1.2 ± 0.4	1.1 ± 0.3	1.0 ± 0.3	0.21
Average reference lumen area (mm^2)	8.5 ± 4.2	9.1 ± 3.5	9.0 ± 4.7	4.5 ± 0.3	8.4 ± 4.4	9.2 ± 5.7	7.6 ± 3.5	9.4 ± 0.9	0.95
Average reference vessel area (mm^2)	13.5 ± 4.1	14.9 ± 2.6	12.9 ± 4.8	8.9 ± 1.8	15.3 ± 6.9	15.2 ± 8.1	15.0 ± 6.2	16.7 ± 4.1	0.34
Average reference plaque burden (%)	42.7 ± 10.2	44.7 ± 9.7	37.8 ± 9.0	46.7 ± 7.1	42.7 ± 10.5	39.9 ± 9.8	44.9 ± 9.7	41.1 ± 11.9	0.98

CSA = cross-sectional area; ISR = in-stent restenosis; MLA = minimum lumen cross-sectional area; NIH = neointimal hyperplasia.

smaller extent of calcium, the most potent single factor inhibiting proper stent expansion.[19]

Lesions with stent fracture or deformation comprised 11% of analyzed SVG ISR and were found exclusively in DES. This corresponds to the data by Inaba et al., who reported IVUS-defined stent fracture or deformation in 9.6% of ISR lesions an average of 1.2 years postimplantation of second generation DES.[12] In the IVUS study by Goto et al.,[13] the frequency of stent fracture was 5% in first-generation DES and 7.4% in second-generation DES, with no stent fracture observed in BMS. The fact that fractures and deformations were confined to DES can be explained by impaired endothelialization and less neointimal hyperplasia leading to reduced mechanical fixation of the stent within the vessel wall.

The present study revealed an association between stent implantation at an SVG anastomosis or hinge motion site and a higher prevalence of mechanical patterns of ISR. Several unique features of anastomotic SVG lesions have been described; graft angulation or scar tissue formation at the suture line may result in suboptimal stent expansion.[20] We hypothesize that SVG anastomoses are also subject to chronic mechanical stress leading to late stent recoil, deformation, or fracture. The same can be true for stents implanted at an SVG hinge motion site. In our study, the average Δ angle was 7.9°, substantially smaller compared with Δ angle reported for native coronary arteries (12° to 20°).[6,21] The mechanism of hinge motion in SVGs may not be solely dependent on the cardiac cycle, but also on formation of fibrotic tissue and vessel adhesion to thoracic structures. In addition, fewer angiographic views are taken in SVGs compared with native arteries potentially leading to underestimation the real Δ angle.

There are several limitations to our analysis. First, this was a retrospective, observational study of only patients with analyzable pre-intervention IVUS; thus, some selection bias must be considered. Second, there are limitations of grayscale IVUS in restenotic tissue characterization and detection of thrombus. Third, BMS were underrepresented in this cohort. Fourth, the majority of initial SVG PCI procedures were performed without imaging guidance, precluding a comparison of procedural and follow-up IVUS images. Fifth, this analysis did not account for the immediate PCI results, including presence of residual stenosis. Sixth, these results should be considered only for SVG and not for arterial conduits.

Finally, the results of our study reinforce the general recommendation to opt for the native vessel treatment in case of SVG failure as well as support the role of routine intravascular imaging guidance in this lesion subset. The use of more resistant stent platforms should be advised for the treatment of SVG lesions located at anastomoses or hinge motion points.

Disclosures

Gary S. Mintz: Consultant - Boston Scientific, ACIST; fellowship/grant support - Philips, Boston Scientific, InfraReDx; honoraria - Boston Scientific, ACIST. Manish A. Parikh: Speakers bureau – Abbott Vascular, Medtronic, Boston Scientific, CSI; advisory board – Abbott Vascular, Medtronic. Ziad A. Ali: Institutional research grants to Columbia University from Abbott and Cardiovascular Systems Inc.; consultant to St Jude Medical, ACIST. Dimitri Karmpaliotis: Speaker's bureau - Abbott Vascular, Boston Scientific. Ajay J. Kirtane: Institutional grants to Columbia University and/or Cardiovascular Research Foundation from Medtronic, Boston Scientific, Abbott Vascular, Abiomed, CSI, CathWorks, Siemens, Philips, ReCor Medical. Jeffrey W. Moses: Consultant: Siemens. Akiko Maehara: Institutional grant support - Boston Scientific, Abbott; consultant - Boston Scientific, OCT Medical Imaging Inc.; speaker fee - Abbott. All other investigators have no disclosures to report.

1. Brilakis ES, O'Donnell CI, Penny W, Armstrong EJ, Tsai T, Maddox TM, Plomondon ME, Banerjee S, Rao SV, Garcia S, Nallamothu B, Shunk KA, Mavromatis K, Grunwald GK, Bhatt DL. Percutaneous coronary intervention in native coronary arteries versus bypass grafts in patients with prior coronary artery bypass graft surgery: insights from the veterans affairs clinical assessment, reporting, and tracking program. *JACC Cardiovasc Interv* 2016;9:884–893.
2. Redfors B, Généreux P, Witzenbichler B, McAndrew T, Diamond J, Huang X, Maehara A, Weisz G, Mehran R, Kirtane AJ, Stone GW. Percutaneous coronary intervention of saphenous vein graft. *Circ Cardiovasc Interv* 2017;10:e004953.
3. Brilakis ES, Edson R, Bhatt DL, Goldman S, Holmes DR, Rao SV, Shunk K, Rangan BV, Mavromatis K, Ramanathan K, Bavry AA, Garcia S, Latif F, Armstrong E, Jneid H, Conner TA, Wagner T, Karacsonyi J, Uyeda L, Ventura B, Alsleben A, Lu Y, Shih M-C, Banerjee S. DIVA Trial Investigators. Drug-eluting stents versus bare-metal stents in saphenous vein grafts: a double-blind, randomised trial. *Lancet* 2018;391:1997–2007.
4. Andalib A, Almonacid A, Popma JJ. Qualitative and quantitative coronary angiography ed).. In: Topol E, ed. Textbook of Interventional Cardiology, 7th ed., Philadelphia: Elsevier; 2016:911–931.
5. Mehran R, Dangas G, Abizaid AS, Mintz GS, Lansky AJ, Satler LF, Pichard AD, Kent KM, Stone GW, Leon MB. Angiographic patterns of in-stent restenosis: classification and implications for long-term outcome. *Circulation* 1999;100:1872–1878.
6. Ino Y, Toyoda Y, Tanaka A, Ishii S, Kusuyama Y, Kubo T, Takarada S, Kitabata H, Tanimoto T, Mizukoshi M, Imanishi T, Akasaka T. Predictors and prognosis of stent fracture after sirolimus-eluting stent implantation. *Circ J* 2009;73:2036–2041.
7. Castagna MT, Mintz GS, Ohlmann P, Kotani J-I, Maehara A, Gevorkian N, Cheneau E, Stabile E, Ajani AE, Suddath WO, Kent KM, Satler LF, Pichard AD, Weissman NJ. Incidence, location, magnitude, and clinical correlates of saphenous vein graft calcification: an intravascular ultrasound and angiographic study. *Circulation* 2005;111:1148–1152.
8. Sonoda S, Morino Y, Ako J, Terashima M, Hassan AHM, Bonneau HN, Leon MB, Moses JW, Yock PG, Honda Y, Kuntz RE, Fitzgerald PJ. Impact of final stent dimensions on long-term results following sirolimus-eluting stent implantation: serial intravascular ultrasound analysis from the sirius trial. *J Am Coll Cardiol* 2004;43:1959–1963.
9. Lee J-B, Mintz GS, Lisauskas JB, Biro SG, Pu J, Sum ST, Madden SP, Burke AP, Goldstein J, Stone GW, Virmani R, Muller JE, Maehara A. Histopathologic validation of the intravascular ultrasound diagnosis of calcified coronary artery nodules. *Am J Cardiol* 2011;108:1547–1551.
10. Maehara A, Mintz GS, Bui AB, Walter OR, Castagna MT, Canos D, Pichard AD, Satler LF, Waksman R, Suddath WO, Laird JR, Kent KM, Weissman NJ. Morphologic and angiographic features of coronary plaque rupture detected by intravascular ultrasound. *J Am Coll Cardiol* 2002;40:904–910.
11. Mintz GS, Nissen SE, Anderson WD, Bailey SR, Erbel R, Fitzgerald PJ, Pinto FJ, Rosenfield K, Siegel RJ, Tuzcu EM, Yock PG, O'Rourke RA, Abrams J, Bates ER, Brodie BR, Douglas PS, Gregoratos G, Hlatky MA, Hochman JS, Kaul S, Tracy CM, Waters DD, Winters WL. ACC Clinical Expert Consensus Document on Standards for the acquisition, measurement and reporting of intravascular ultrasound studies: a report of the American College of Cardiology Task Force on Clinical Expert Consensus Documents (Committee to Develop a Clinical Expert Consensus Document on Standards for Acquisition,

Measurement and Reporting of Intravascular Ultrasound Studies [IVUS]). *J Am Coll Cardiol* 2001;37:1478–1492.
12. Inaba S, Mintz GS, Yun KH, Yakushiji T, Shimizu T, Kang S-J, Généreux P, Weisz G, Rabbani LE, Moses JW, Stone GW, Maehara A. Mechanical complications of everolimus-eluting stents associated with adverse events: an intravascular ultrasound study. *Eurointervention* 2014;9:1301–1308.
13. Goto K, Zhao Z, Matsumura M, Dohi T, Kobayashi N, Kirtane AJ, Rabbani LE, Collins MB, Parikh MA, Kodali SK, Leon MB, Moses JW, Mintz GS, Maehara A. Mechanisms and patterns of intravascular ultrasound in-stent restenosis among bare metal stents and first- and second-generation drug-eluting stents. *Am J Cardiol* 2015;116:1351–1357.
14. Kang S-J, Mintz GS, Park D-W, Lee S-W, Kim Y-H, Lee CW, Han K-H, Kim J-J, Park S-W, Park S-J. Mechanisms of in-stent restenosis after drug-eluting stent implantation: intravascular ultrasound analysis. *Circ Cardiovasc Interv* 2011;4:9–14.
15. Kang S-J, Mintz GS, Park D-W, Lee S-W, Kim Y-H, Lee CW, Han K-H, Kim J-J, Park S-W, Park S-J. Tissue characterization of in-stent neointima using intravascular ultrasound radiofrequency data analysis. *Am J Cardiol* 2010;106:1561–1565.
16. Nakazawa G, Otsuka F, Nakano M, Vorpahl M, Yazdani SK, Ladich E, Kolodgie FD, Finn AV, Virmani R. The pathology of neoatherosclerosis in human coronary implants: bare-metal and drug-eluting stents. *J Am Coll Cardiol* 2011;57:1314–1322.
17. Song L, Mintz GS, Yin D, Yamamoto MH, Chin CY, Matsumura M, Kirtane AJ, Parikh MA, Moses JW, Ali ZA, Shlofmitz RA, Maehara A. Characteristics of early versus late in-stent restenosis in second-generation drug-eluting stents: an optical coherence tomography study. *Eurointervention* 2017;13:294–302.
18. Jensen LO, Vikman S, Antonsen L, Kosonen P, Niemelä M, Christiansen EH, Kervinen K, Erglis A, Harnek J, Kumsars I, Thuesen L, Niemelä K. Intravascular ultrasound assessment of minimum lumen area and intimal hyperplasia in in-stent restenosis after drug-eluting or bare-metal stent implantation. The Nordic Intravascular Ultrasound Study (NIVUS). *Cardiovasc Revasc Med* 2017;18:577–582.
19. Kobayashi Y, Okura H, Kume T, Yamada R, Kobayashi Y, Fukuhara K, Koyama T, Nezuo S, Neishi Y, Hayashida A, Kawamoto T, Yoshida K. Impact of target lesion coronary calcification on stent expansion. *Circ J* 2014;78:2209–2214.
20. Sano K, Mintz GS, Carlier SG, Fujii K, Yasuda T, Kimura M, Costa JR, Costa RA, Lui J, Weisz G, Moussa I, Dangas GD, Mehran R, Lansky AJ, Kreps EM, Collins M, Stone GW, Moses JW, Leon MB. Intravascular ultrasonic differences between aorto-ostial and shaft narrowing in saphenous veins used as aortocoronary bypass grafts. *Am J Cardiol* 2006;97:1463–1466.
21. Ino Y, Kubo T, Kitabata H, Shimamura K, Shiono Y, Orii M, Okochi K, Sougawa H, Tanimoto T, Komukai K, Ishibashi K, Takarada S, Nakanishi H, Tanaka A, Kimura K, Hirata K, Mizukoshi M, Imanishi T, Akasaka T. Impact of hinge motion on in-stent restenosis after sirolimus-eluting stent implantation. *Circ J* 2011;75:1878–1884.